Critical role of aquaporin-4 (AQP4) in astrocytic Ca^{2+} signaling events elicited by cerebral edema

Alexander S. Thrane[a,b,c,1], Phillip M. Rappold[a,1], Takumi Fujita[a,1], Arnulfo Torres[a], Lane K. Bekar[a], Takahiro Takano[a], Weiguo Peng[a], Fushun Wang[a], Vinita Rangroo Thrane[a,b,c], Rune Enger[b,c], Nadia N. Haj-Yasein[b,c], Øivind Skare[d,e], Torgeir Holen[f], Arne Klungland[g], Ole P. Ottersen[b,2], Maiken Nedergaard[a,2], and Erlend A. Nagelhus[a,b,c,h,2]

[a]Division of Glial Disease and Therapeutics, Center for Translational Neuromedicine, Department of Neurosurgery, University of Rochester Medical Center, Rochester, NY 14642; [b]Centre for Molecular Biology and Neuroscience, Letten Centre, Institute of Basic Medical Sciences, University of Oslo, 0317 Oslo, Norway; [c]Centre for Molecular Medicine Norway, Nordic European Molecular Biology Laboratory Partnership, University of Oslo, 0318 Oslo, Norway; [d]Division of Epidemiology, Norwegian Institute of Public Health, 0403 Oslo, Norway; [e]Department of Public Health and Primary Health Care, University of Bergen, 5020 Bergen, Norway; [f]Department of Anatomy, Institute of Basic Medical Sciences, University of Oslo, 0317 Oslo, Norway; [g]Centre for Molecular Biology and Neuroscience, Institute of Medical Microbiology, Oslo University Hospital, 0027 Oslo, Norway; and [h]Department of Neurology, Oslo University Hospital, 0027 Oslo, Norway

Edited* by Peter Agre, The Johns Hopkins Malaria Research Institute, Baltimore, MD, and approved December 6, 2010 (received for review October 14, 2010)

Aquaporin-4 (AQP4) is a primary influx route for water during brain edema formation. Here, we provide evidence that brain swelling triggers Ca^{2+} signaling in astrocytes and that deletion of the Aqp4 gene markedly interferes with these events. Using in vivo two-photon imaging, we show that hypoosmotic stress (20% reduction in osmolarity) initiates astrocytic Ca^{2+} spikes and that deletion of *Aqp4* reduces these signals. The Ca^{2+} signals are partly dependent on activation of P2 purinergic receptors, which was judged from the effects of appropriate antagonists applied to cortical slices. Supporting the involvement of purinergic signaling, osmotic stress was found to induce ATP release from cultured astrocytes in an AQP4-dependent manner. Our results suggest that AQP4 not only serves as an influx route for water but also is critical for initiating downstream signaling events that may affect and potentially exacerbate the pathological outcome in clinical conditions associated with brain edema.

endfeet | glial | two-photon

Using in vivo two-photon imaging of mice subjected to hypoosmotic stress, we have shown previously that astrocytes rapidly swell in the initial phase of edema development (1). These data are consistent with a number of studies suggesting that aquaporin-4 (AQP4) serves as a primary influx route for water from blood to brain (2, 3). AQP4 is strongly expressed in astrocytic endfeet (4), which form a continuous pericapillary sheath that is interrupted only by a narrow extracellular space (5).

In vitro studies clearly show that swelling of astrocytes leads to the activation of a number of signaling cascades (6, 7). Because astrocytes are prone to swell in experimental conditions associated with edema formation (8), this raises the question of whether the same signaling cascades are activated in early edema formation in vivo and whether they affect the clinical outcome.

Hypoosmotic stress induces brain edema with early accumulation of water in astrocytes (1, 9, 10). Thus, hypoosmotic stress provides a suitable experimental model to explore potential signaling mechanisms initiated by astrocytic swelling in vivo. Here, we use optical imaging to show that hypoosmotic stress induces Ca^{2+} spikes in astrocytes in vivo and that these spikes are potentiated in the presence of AQP4. We also provide in vitro data indicating that the AQP4-dependent Ca^{2+} signals are mediated in part by autocrine purinergic signaling. Our findings show that brain edema formation should not be seen merely as a process of passive water accumulation in brain but as a condition that sets in motion specific signaling processes that may significantly affect disease progression and morbidity.

Results

***Aqp4* Deletion Reduces Swelling of Cortical Astrocytes Exposed to Mild Hypoosmotic Stress.** Immunofluorescence and Western blots confirmed the efficacy of the $Aqp4^{-/-}$ KO strategy (Fig. 1 *A* and *B*). Light microscopy revealed normal cytoarchitecture of cortex in $Aqp4^{-/-}$ mice. Specifically, astrocytes, visualized by GFAP immunolabeling, displayed normal morphology and intact endfeet (Fig. 1*B*).

To further validate the *Aqp4* deletion, we performed volumetric analysis of astrocytic somata in acute cortical slices exposed to solution of reduced osmolarity (Fig. 1*C*). Astrocytes were readily detected by two-photon imaging after the slice had been incubated with the fluorescent dye Texas red hydrazide, an approach similar to that described for sulphorhodamine 101 (11, 12). Dye loading of slices obtained from transgenic mice that express EGFP under control of the *Glt-1* promoter (*Glt-1*–EGFP BAC transgenic mice) (13) confirmed that Texas red hydrazide was selectively taken up by GFP-expressing astrocytes (Fig. 1*D*).

When exposed to 20% reduction in osmolarity, WT astrocytes exhibited a peak increase in soma volume of $19 \pm 1.2\%$ after 5 min, which was significantly higher than the $3 \pm 0.8\%$ increase observed in $Aqp4^{-/-}$ astrocytes ($P < 0.001$, two-tailed Student *t* test) (Fig. 1*E*). In both genotypes, the initial swelling was followed by a nearly linear volume reduction, reflecting regulatory volume decrease.

To explore whether volume recovery was dependent on the magnitude of osmotic stress, we exposed WT and $Aqp4^{-/-}$ astrocytes to artificial cerebrospinal fluid (aCSF) with 30% reduction in osmolarity. Under this condition, astrocytes from both genotypes showed continuous increase in soma volume, and magnitude of swelling was similar (Fig. 1*E*).

Hypoosmotic Stress Enhances Ca^{2+} Signals in Cortical Layer 1 Astrocytes in Vivo. In vivo two-photon imaging of *Glt-1*–EGFP BAC transgenic mice confirmed that the Ca^{2+} indicator Rhod2 AM was taken up by astrocytes (Fig. 2 *A* and *B*). Increase in Rhod2 signal intensity was not associated with altered GFP signal (Fig. 2*B*). The ratio between Rhod2 and GFP signal intensities provided a more reliable measure of astrocytic Ca^{2+} signals than the Rhod2 signal (Fig. 2*C*), reflecting that the former measure is less sensitive to inadvertent small shifts in focal plane. In neither WT nor $Aqp4^{-/-}$ mice did frequency of astrocytic Ca^{2+} spikes change over time in the control state (0.092 ± 0.038 vs. 0.197 ± 0.065 for the first and last 15 min in WT, $n = 76$

Author contributions: A.S.T., P.M.R., T.F., A.T., L.K.B., T.T., M.N., and E.A.N. designed research; A.S.T., P.M.R., T.F., A.T., L.K.B., W.P., F.W., R.E., N.N.H.-Y., and E.A.N. performed research; L.K.B., T.T., T.H., A.K., O.P.O., M.N., and E.A.N. contributed new reagents/analytic tools; A.S.T., P.M.R., T.F., V.R.T., Ø.S., and E.A.N. analyzed data; and A.S.T., P.M.R., O.P.O., M.N., and E.A.N. wrote the paper.

The authors declare no conflict of interest.

*This Direct Submission article had a prearranged editor.

Freely available online through the PNAS open access option.

[1]A.S.T., P.R., and T.F. contributed equally to this work.

[2]To whom correspondence may be addressed. E-mail: oleppp@yahoo.com, nedergaard@urmc.rochester.edu, or e.a.nagelhus@ncmm.uio.no.

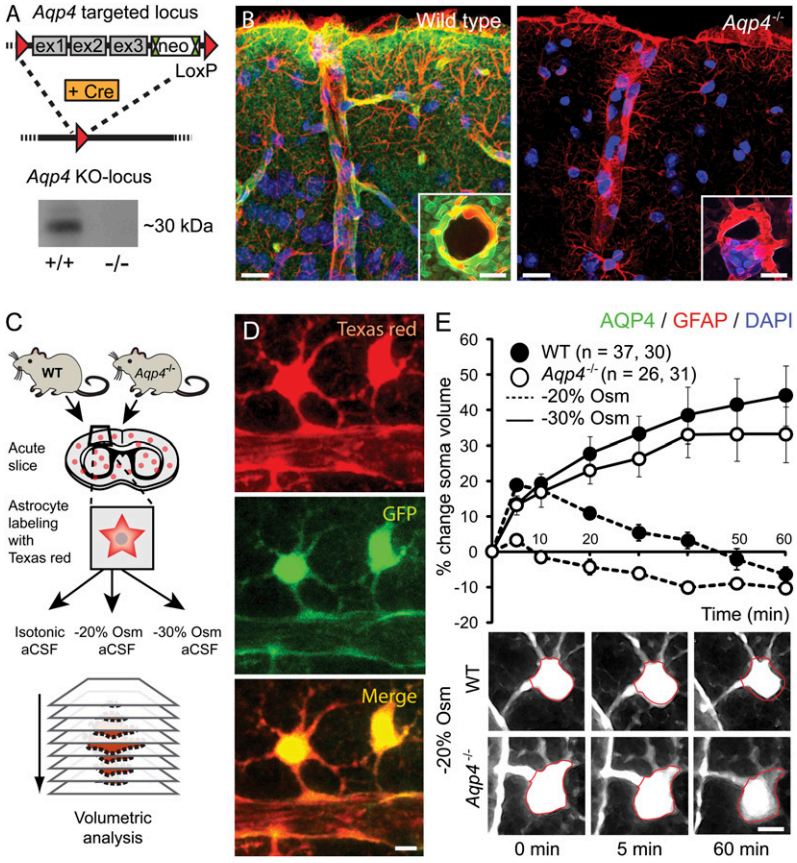

Fig. 1. *Aqp4* KO strategy and validation. (*A*) The targeted allele contained a flippase recognition target (FRT)-neomycin-FRT cassette after exon 3 and LoxP sites upstream and downstream of exons 1–3. Floxed mice were bred with Cre-expressing mice to produce mice with the *Aqp4* KO allele. Western blot confirmed the absence of AQP4 in $Aqp4^{-/-}$ mice. (*B*) Immunofluorescence micrographs of mouse cortex probed with primary antibodies against AQP4 (green) and GFAP (red) with DAPI-labeled nuclei (blue) for orientation. The AQP4 immunofluorescence signal is absent in $Aqp4^{-/-}$ mice. *Insets* display perivascular AQP4 and GFAP labeling at higher magnification. (Scale bar: 25 μm; *Inset*, 5 μm.) (*C*) Experimental design for validating the effect of *Aqp4* deletion on osmotically induced astrocyte swelling. Acute brain slices were prepared from WT and $Aqp4^{-/-}$ mouse pups. Slices were loaded with Texas red hydrazide and perfused with aCSF with normal (isotonic) or reduced osmolarity (−20% or −30% Osm). Sectional images were acquired for 3D volume analysis. (*D*) Two-photon imaging of Texas red hydrazide-loaded slices obtained from mice expressing GFP in astrocytes (*Glt-1*–EGFP BAC transgenic mice) confirmed that the dye was selectively taken up by astrocytes. (Scale bar: 5 μm.) (*E*) Exposure of acute cortical slices to 20% reduction in osmolarity (−20% Osm) induced more prominent swelling of astrocytic somata in WT ($n = 37$) than in $Aqp4^{-/-}$ mice ($n = 26$; $P < 0.001$ at 5 min, two-tailed Student t test). The initial swelling was followed by shrinkage reflecting regulatory volume decrease. More severe osmotic stress (−30% Osm) induced continuous swelling in both genotypes ($n = 30$ and 31). Error bars represent SEM. *Lower* shows representative images of astrocytes exposed to −20% Osm. The red ring marks the astrocyte soma circumference at baseline. (Scale bar: 5 μm.)

cells, $P = 0.15$; 0.179 ± 0.111 vs. 0.232 ± 0.076 in $Aqp4^{-/-}$, $n = 56$, $P = 0.55$; mixed model analyses) (*Methods*).

Brain edema induced by i.p. water injection was associated with enhanced Ca^{2+} signals in WT mice (Fig. 2 *D*–*G*). Frequency of astrocytic Ca^{2+} spikes and percentage of astrocytes with Ca^{2+} spikes (active cells) increased already in the first 15-min period post water injection and became even higher as brain swelling progressed (Fig. 2*G*). Spike amplitude and proportion of long-lasting (≥30 s) spikes also became higher in the late phase of osmotic brain edema (Fig. 2 *E* and *F*).

Osmotically Induced Astrocytic Ca^{2+} Spikes in Vivo Are Dependent on AQP4. In the control state, frequency of astrocytic Ca^{2+} spikes did not differ between WT and $Aqp4^{-/-}$ mice ($P = 0.69$) (Fig. 2*G*). In contrast to WT, $Aqp4^{-/-}$ mice did not respond to water injection with altered astrocytic spike frequency (Fig. 2*G*). Only the proportion of active astrocytes increased somewhat in the late phase of osmotic brain swelling (Fig. 2*G*). At this stage, proportion of active astrocytes ($P = 0.0042$) and spike frequency ($P = 0.0038$) differed between WT and $Aqp4^{-/-}$ mice. In the first 15 min after water injection, these values did not differ significantly between genotypes ($P = 0.098$ and $P = 0.159$, respectively; mixed model analyses) (*Methods*), probably reflecting the time it takes for brain swelling to develop after i.p. water injection.

Mild Hypoosmotic Stress Induces AQP4-Dependent Astrocytic Ca^{2+} Responses in Acute Cortical Slices. Supporting our in vivo findings, we found that exposing acute cortical slices to mild hypoosmotic aCSF (20% reduction in osmolarity) robustly triggered astrocytic Ca^{2+} spikes in WT mice (Fig. 3 *A* and *B*). The proportion of astrocytes that responded with Ca^{2+} spikes was much lower in $Aqp4^{-/-}$ than in WT mice (Fig. 3 *A* and *B*). Moreover, Ca^{2+} spikes in $Aqp4^{-/-}$ mice had a lower amplitude (Fig. 3*B*) and delayed onset (272 ± 9 s in $Aqp4^{-/-}$ vs. 162 ± 4 s in WT, $P < 0.001$, two-tailed Student t test). More severe osmotic stress (30% reduction in osmolarity) diminished the difference in responder rate between WT and $Aqp4^{-/-}$ mice (Fig. 3*B*), possibly reflecting robust astrocyte swelling in both genotypes during this condition (compare with Fig. 1*E*). However, at 30% reduction in osmolarity, the spike amplitude was still lower in $Aqp4^{-/-}$ than in WT mice (Fig. 3*B*).

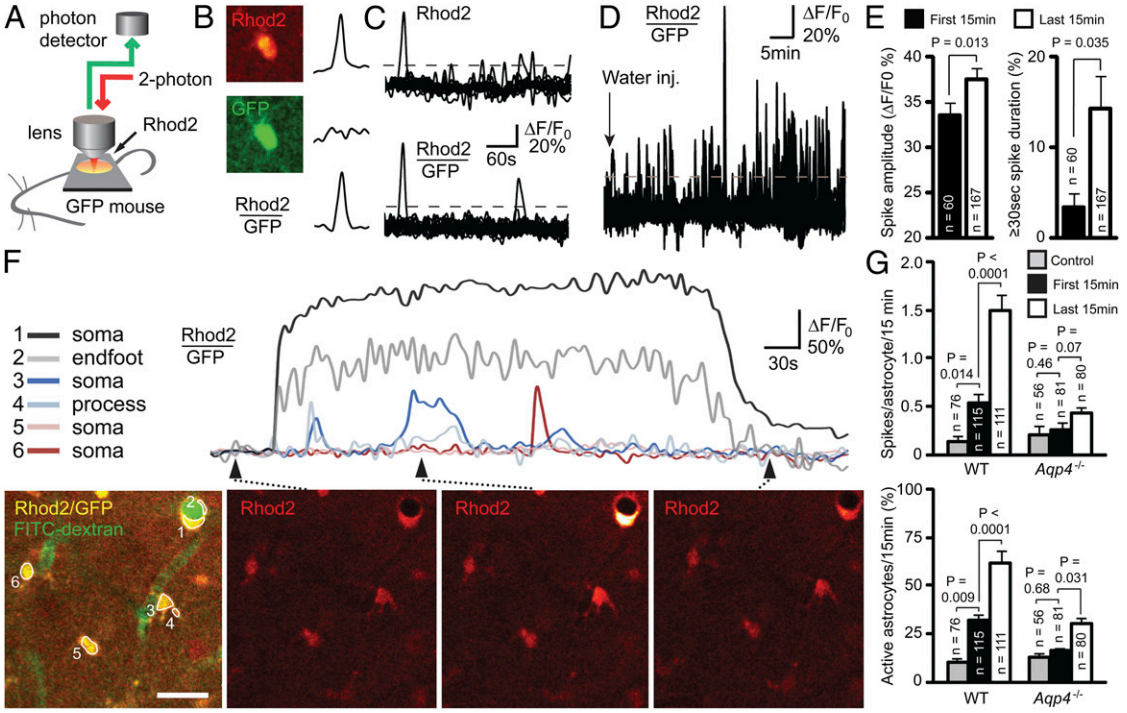

Fig. 2. In vivo two-photon imaging of astroglial Ca^{2+} signals during hypoosmotic stress. (*A*) Diagram of experimental setup. Astrocytic Ca^{2+} transients were detected in anesthetized *Glt-1*–EGFP BAC transgenic mice after loading of Rhod2 AM onto the cortical surface. (*B*) Images show Rhod2 fluorescence in a GFP-expressing astrocyte. Because increase in Rhod2 signals were not associated with changes in GFP fluorescence, the ratio between the two signals provided a measure of the astrocytic Ca^{2+} signal. (*C*) During brain swelling, the ratio between Rhod2 and GFP fluorescent signal intensities (lower trace) was less sensitive to inadvertent small shifts in focal plane than Rhod2 signals (upper trace). Thus, Rhod2/GFP signals were used for reliably defining Ca^{2+} spikes [i.e., transients exceeding 20% (dashed line) of baseline]. (*D*) Pooled Ca^{2+} traces (measured as relative changes in Rhod2/GFP) for all astrocytes ($n = 24$) within an image field in a WT mouse subjected to i.p. water injection (indicated by arrow; 200 mL/kg) to induce osmotic brain swelling. Note increase in spike frequency and amplitude as brain edema develops. (*E*) In WT mice, relative spike amplitude and proportion of spikes lasting ≥30 s were higher in the last 15 min than in the first 15 min after water injection. (*F*) Traces of relative Ca^{2+} changes in WT astrocytes 30 min after i.p. water injection. The position of the respective astrocytes (confluent Rhod2 and GFP signals in yellow) is indicated in *Left*. FITC-dextran (green) was injected i.v. at the beginning of the experiment to outline the vasculature, and it confirmed vascular perfusion. Time-lapse sequence of the Ca^{2+} responses is shown in *Right*. Note the intense and long-lasting Ca^{2+} surge in the astrocytic soma and endfoot surrounding a vein. (Scale bar: 25 μm.) (*G*) In WT mice, the frequency of astrocytic Ca^{2+} spikes was higher already in the first 15 min after water injection compared with the control state, and it was even higher in the last 15 min of observation. In $Aqp4^{-/-}$ mice, water injection did not increase spike frequency. The percentage of astrocytes with more than or equal to one Ca^{2+} spike(s) per 15-min observation (active astrocytes) increased profoundly in WT mice after water injection. In $Aqp4^{-/-}$ mice, the number of active astrocytes increased only at the late phase of osmotic brain swelling. Error bars represent SEM. Mixed model analyses were performed using a binomial (Bernoulli) model with logit link for binary observations (passive or active cells), a Poisson model for count data (spike frequency), and a linear model for spike amplitudes (24).

AQP4-Dependent Ca^{2+} Signals Are Mediated in Part by Autocrine Purinergic Signaling. Incubating WT slices with the nonselective P2 antagonists suramin and pyridoxal-phosphate-6-azophenyl-2′,4′-disulfonate (PPADS) delayed onset of Ca^{2+} responses to mild hypoosmotic stress (327 ± 8 s vs. 241 ± 9 s without antagonists, $P < 0.001$, two-tailed Student t test) and reduced percentage of responding astrocytes (Fig. 3*B*). Microinjection of ATP in cortical slices induced astrocytic Ca^{2+} responses with similar kinetics in WT and $Aqp4^{-/-}$ mice (Fig. 3*B Lower*) (mean amplitude = 68 ± 2% vs. 69 ± 3%; time to response = 11 ± 1.2 s vs. 12 ± 1.2 s, respectively), suggesting that *Aqp4* deletion did not interfere with signaling mechanisms downstream of purinergic receptor activation.

***Aqp4* Deletion Abrogates Osmotically Induced ATP Release from Cultured Astrocytes.** Cultured WT astrocytes exposed to hypoosmotic medium (−20% Osm) for 15 min released more ATP than those kept in isotonic solution (Fig. 3*C*). In contrast, cultured $Aqp4^{-/-}$ astrocytes subjected to similar stress showed no significant change in ATP release (Fig. 3*C*). Taken together, our data are compatible with a role for AQP4 in amplifying signaling events triggered by cell swelling (Fig. 3*D*).

Discussion

Brain edema formation is commonly regarded as a passive process by which water accumulates in the brain because of changes in osmotic driving forces or perturbations of the blood–brain barrier. Hence, the symptomatology and treatment of this serious condition is usually discussed in the context of the accompanying intracranial pressure changes that may eventually cause herniation and compromise blood flow to the brain. The possibility that brain edema formation sets in motion pathophysiologically relevant signaling processes has largely been overlooked. This is remarkable given the fact that cell swelling—the hallmark of cytotoxic edema—is known to activate a number of signaling cascades that may have profound effects on cell function (14). Specifically, in vitro studies have shown that swelling causes astrocytes to release neuroactive substances such as glutamate and ATP (6, 15).

This study shows that incipient edema is associated with astrocytic Ca^{2+} signals in vivo. These signals are causally linked to water influx and cell swelling, because they were significantly reduced in animals deficient in AQP4. Previously, deletion of *Aqp4* has been shown to abrogate osmotically induced astrocytic swelling and counteract build-up of brain edema (8, 16).

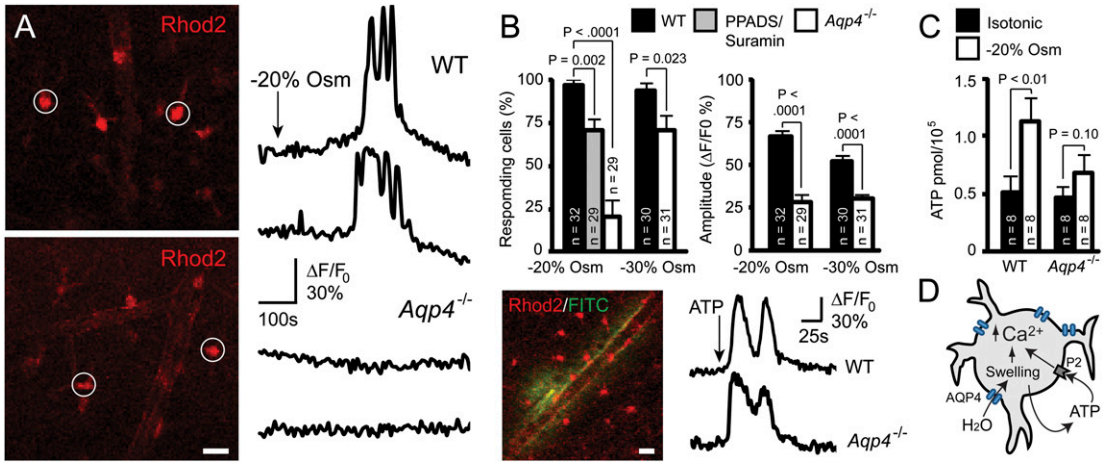

Fig. 3. Osmotically induced astrocytic Ca^{2+} responses and ATP release in vitro. (*A*) Two-photon images of Rhod2 AM-loaded acute cortical slices obtained from WT (*Upper*) and *Aqp4*$^{-/-}$ (*Lower*) mice. Traces shown are from astrocytes marked in *Left*. Exposure of slices from WT mice to aCSF with 20% reduction in osmolarity (−20% Osm) induced brisk astrocytic Ca^{2+} spikes. In contrast, this osmotic stress failed to elicit Ca^{2+} spikes in most AQP4-deficient astrocytes. (*B*) Quantitative analysis of astrocytic Ca^{2+} responses to osmotic stress. Deletion of *Aqp4* or blocking P2 purinergic receptors with PPADS/suramin significantly reduced the number of astrocytes that responded with Ca^{2+} spikes during exposure to −20% Osm. When more severe hypoosmotic stress (−30% Osm) was applied, a larger fraction of the *Aqp4*$^{-/-}$ astrocytes responded. The amplitude of the Ca^{2+} spikes differed between the genotypes for both types of stress. Image shows intense Ca^{2+} signals in Rhod2-loaded astrocytes after microinjection of ATP and FITC-dextran (green; to verify injection) into the slice. Representative traces from WT and *Aqp4*$^{-/-}$ mice are shown. (*C*) Cultured astrocytes exposed to hypoosmotic media (−20% Osm, 15 min) released significantly more ATP than those kept in isotonic media. Astrocytes from *Aqp4*$^{-/-}$ mice did not show osmotically induced ATP release. *P* values were obtained by two-tailed Student *t* test. Error bars represent SEM. (Scale bar: 25 μm.) (*D*) Diagram showing proposed involvement of AQP4 in astrocyte signaling cascades during hypoosmotic stress. AQP4-mediated water influx triggers Ca^{2+} transients, partly by promoting release of ATP and activation of P2 purinergic receptors.

The in vivo analyses were complemented with monitoring of blood flow in the microvascular bed. Despite absence of overt changes, it is difficult to rule out small alterations in cerebral perfusion caused by the incipient brain edema. Thus, it was deemed necessary to include complementary in vitro studies in slices. Such studies also allowed us to dissect the mechanisms underlying the AQP4-sensitive Ca^{2+} responses. Analyses in acute cortical slices supported the data obtained in vivo. Notably, slices exposed to hypoosmotic media displayed Ca^{2+} signals in astrocytes reminiscent of those seen in vivo. These signals were attenuated after *Aqp4* deletion. The attenuation was particularly pronounced at 20% decrease in osmolarity.

Previous in vitro studies have shown that activation of purinergic receptors triggers astrocytic Ca^{2+} transients (17–19). We hypothesized that Ca^{2+} signals elicited during edema formation depend—at least in part—on ATP release from swollen astrocytes. Application of P2 antagonists to acute cortical slices supported this view. The quantitative analysis indicated that, in ∼25% of WT astrocytes, the Ca^{2+} response was contingent on ATP signaling. Obviously, additional mechanisms are at play and contribute to the observed Ca^{2+} signals. Stretch-sensitive receptors are likely to be among these mechanisms.

Next, we set out to resolve whether astrocytes could serve as a source of ATP. In cultured astrocytes, osmotic stress induced ATP release, and this release was abolished after *Aqp4* deletion. Taken together, the data suggest that AQP4 not only mediates water influx but also is essential for initiating signaling events associated with edema formation. This may explain the rather pronounced protective effect of *Aqp4* KO or AQP4 mislocalization in stroke models (8, 20). It is well-known that water passes through the lipid bilayer of the plasma membrane (although to a limited extent compared with the water flux through aquaporin channels) and that diffusion also occurs through the thin slits that separate the astrocyte endfeet. In AQP4-deficient mice, a discrepancy between the extent of water transport restriction on the one hand and the protective effect in stroke on the other hand can easily be explained if loss of AQP4 also interferes with signaling mechanisms that exacerbate the pathological outcome.

Edema formation and cytotoxicity likely engage in a vicious cycle, where cell swelling causes release of cytotoxic compounds that, in turn, lead to tissue damage and more swelling. ATP is known to act as a cytotoxic compound in stroke, as judged by a number of in vitro and in vivo studies (21). Thus, an early-stage intervention with AQP4 inhibitors would interfere with this vicious cycle by counteracting not only the swelling per se but also deleterious secondary events like ATP release. Further studies are required to resolve whether AQP4 is also involved in swelling-activated glutamate efflux through volume-sensitive channels (6).

An obvious question is whether the effect of *Aqp4* deletion solely depends on the change in swelling response or whether AQP4 (alone or in combination with other molecules) serves as an osmosensor upstream of the above signaling events. To distinguish between these possibilities, we exposed acute slices to an osmotic stress (30% reduction in osmolarity) severe enough to override the mechanisms that normally limit transmembrane water transport, as evidenced by the reduced sensitivity to *Aqp4* deletion. With an osmotic stress at this scale, the percentage of astrocytes that responded with Ca^{2+} spikes was nearly as high in the *Aqp4*$^{-/-}$ animals as in WT. This observation is consistent with the idea that the Ca^{2+} signals are elicited by the AQP4-induced swelling response rather than through an osmoreceptor response.

Conclusion

Our study has revealed that induction of brain edema sets in motion specific signaling events in brain cells. Notably, we have shown by in vivo two-photon imaging that osmotic stress and edema formation are associated with brisk Ca^{2+} signals in cortical astrocytes. This observation prompted us to resolve whether these signals are dependent on AQP4, which is assumed to constitute the main influx route for water at the brain–blood interface. Using a *Aqp4*$^{-/-}$ line, we show that deletion of *Aqp4* interferes with the frequency and amplitude as well as the duration of the Ca^{2+} signals observed. Taken together with complementary analyses in reduced experimental models, our data are consistent with the idea that AQP4-mediated cell swelling is inextricably coupled with activation of signaling pathways that

may profoundly affect the pathological and pathophysiological outcome in clinical conditions associated with brain edema.

Methods

Mice. *Aqp4*$^{-/-}$ mice were generated by GenOway by cloning and sequencing of a targeted region of the murine *Aqp4* gene in a 129/Sv genetic background. The strategy was to design a targeted locus allowing us to delete exons 1–3 to avoid any expression of putative splice variants. Hence, a flippase recognition target (FRT)-neomycin-FRT-LoxP–validated cassette was inserted downstream of exon 3, and a LoxP site was inserted upstream of exon 1 as depicted in Fig. 1*A*. After homologous recombination in ES cells, ES-cell injection into blastocytes, and generation of chimeras, heterozygous floxed mice were obtained by breeding chimeras with C57BL/6J females. Heterozygous floxed mice were bred with C57BL/6J Cre expressing mice to generate mice heterozygous for the KO allele, *Aqp4*$^{+/-}$. The *Aqp4*$^{+/-}$ mice were then backcrossed with C57BL/6J mice for five generations before intercrossing to yield *Aqp4*$^{-/-}$ and *Aqp4*$^{+/+}$ (WTs). For acute cortical slice experiments, we also used C57BL/6J pups from Jackson Laboratory as WT controls. For in vivo experiments, we used *Aqp4*$^{-/-}$ and WT mice expressing EGFP in astrocytes. These mice were generated by breeding *Aqp4*$^{-/-}$ and WT mice with BAC promoter reporter transgenic mice that express EGFP under the control of the natural *Glt-1* promoter (13). The latter mice were provided by J. D. Rothstein (Johns Hopkins University, Baltimore, MD).

Western Blot and Immunohistochemistry. After homogenization and solubilization, extracts of *Aqp4*$^{-/-}$ and WT brains were loaded onto a 10% SDS/PAGE gel and subsequently transferred onto 0.2-μm poly(vinylidene difluoride) membrane (Bio-Rad). The membrane was probed with 0.02 μg/mL goat anti-AQP4 (Cat# sc-9888; Santa Cruz Biotechnology), developed using alkaline phosphatase substrate (ECF Western blotting reagents; Amersham Pharmacia), and visualized with a Typhoon Variable Mode Imager (Amersham Pharmacia). Fixation of mice, preparation of tissue slices, and immunohistochemistry were performed as described previously (22). We used a monoclonal antibody against GFAP (G3893, 1:100; Sigma) and a polyclonal antibody against AQP4 (AB3068, 1:100; Chemicon International).

Animal Preparation for in Vivo Imaging. Eight- to twelve-wk-old WT and *Aqp4*$^{-/-}$ mice expressing EGFP in astrocytes were anesthetized with urethane and α-chloralose (1 g/kg and 50 mg/kg i.p., respectively), intubated, and artificially ventilated with room air using a small animal ventilator (SAR830; CWE) set to ∼100 breaths/min with a tidal volume of 0.3–0.4 mL. Body temperature was kept at 37 °C by a temperature-controlled heating blanket. A craniotomy (3 mm in diameter) was made over the cortex 1 mm lateral and 0.5 mm posterior to the bregma, and the dura was removed. The Ca^{2+} indicator Rhod2 AM (2 mM; Invitrogen) was loaded to the exposed cortex for ∼50 min. After washing for 10 min with aCSF, the craniotomy was covered with 1% agarose in aCSF and sealed by a coverslip. The femoral artery was cannulated for continuous monitoring of mean arterial blood pressure and analysis of blood gases. Only mice with blood gases within the physiological range (pO_2 = 80–150 mmHg, pCO_2 = 30–45 mmHg, pH 7.25–7.5) were included. To outline the vasculature, we administered FITC-dextran (2,000 kDa, ∼0.4 mL, 2.5% in saline; Sigma) intravenously. WT and *Aqp4*$^{-/-}$ mice (n = 6 for each genotype) were injected with distilled water (200 mL/kg) i.p. immediately before imaging. Mice not receiving water injections (n = 3 for each genotype) served as controls.

In Vivo Two-Photon Imaging. A Mai Tai laser (SpectraPhysics) attached to a confocal scanning system (Fluoview 300; Olympus) and an upright microscope (IX51W; Olympus) was used for in vivo imaging, as previously described (23). A 20× (0.9 NA) water immersion lens with 3× additional zoom was used to image astrocytes in cortical layer 1. Excitation wavelength was 860 nm, and emission was collected at 575–645 nm. Dual-channel (Rhod2 and GFP) images with 512 × 512-pixel frames were acquired in a region with intact capillary perfusion every 5 s for 60 min or until capillary perfusion stopped. The low sampling rate was used to avoid photo damage. The two-photon laser power was adjusted to a power that was less than 40 mW at the sample. Two of six WT and one of six *Aqp4*$^{-/-}$ mice subjected to water injection died before 60 min (at 30, 48, and 55 min, respectively). During brain swelling, the focus was adjusted for persistent imaging of the same area. A Ca^{2+} spike was defined when the relative ratio between the Rhod2 and GFP signal intensities exceeded 20% of baseline over a 10-min recording period. Frequency of spikes was calculated per astrocyte per 15 min. Because of the low frequency of Ca^{2+} spikes in the control state, we averaged data for two consecutive 15-min periods. Active astrocytes were defined as cells that had more than or equal to one Ca^{2+} spike(s) per 15 min. Values are expressed as mean ± SEM. Mixed model analyses were performed using a binomial (Bernoulli) model with logit link for binary observations (passive or active cells), a Poisson model for count data (spike frequency), and a linear model for spike amplitudes (24). A hierarchical structure was assumed for all these models, with random effects representing variation between animals and cells inside animals. All experiments were approved by the Institution Animal Care and Use Committee of University of Rochester.

Preparation of Acute Cortical Slices and Dye Loading. Coronal cortical slices were prepared from 10- to 20-d-old mice of either sex as described previously (22, 25). In brief, the brains were submerged in gassed (95% O_2 and 5% CO_2) ice-cold cutting solution, and coronal slices (400 μm) were cut on a Vibratome (TPI). Slices were incubated for 20 min in aCSF and then loaded with either Rhod2 AM (2 mM) or Texas red hydrazide (1.5 μM) in aCSF at 35 °C for 50 min. The aCSF, gassed as described above, contained (in mM) 126 NaCl, 2.5 KCl, 1.25 NaH_2PO_4, 2 $MgCl_2$, 2 $CaCl_2$, 10 glucose, and 26 $NaHCO_3$ (pH 7.4).

Two-Photon Imaging in Acute Cortical Slices. Dye-loaded slices were transferred to a recording chamber (1.5 mL), held in place by a nylon-threaded metal grid, and continuously perfused with aCSF (room temperature) at a rate of 2 mL/min. A multiphoton laser scanning microscope as described above was used for imaging (excitation wavelength = 820–860 nm; emission collected at 575–645 nm). A 60× (0.9 NA) water immersion lens with 6–10× additional zoom was used for the volume assessment, whereas a 20× (0.9 NA) water immersion lens was used for calcium imaging. All experiments were performed at room temperature. After imaging in normal aCSF, we switched the perfusion solution to hypoosmotic aCSF. This solution differed from the control aCSF only with respect to the NaCl concentration, which was either reduced by 20% or 30% (NaCl = 100.8 or 88.2 mM, respectively). Osmolarities were verified by freezing-point depression.

Volumetry. Astrocytes with endfeet visibly extending to vessels at a tissue depth >40 μm were selected, and 3D image stacks were collected; frame sizes of 256 × 256 at intervals of 1.5–3.0 μm in the z direction were collected with an acquisition time of <20 s using minimal laser power (<40 mW). Images were acquired for a 60-min period and then analyzed for changes in soma volume using custom-made software (Matlab Inc.). A median filter with a radius of 5 pixels was used to reduce background noise. A region of interest was defined around the soma in maximum intensity projections using fixed landmarks for all time points within an experiment. Pixels over a certain threshold within this region were counted for each xy frame in the z stack. Laser power, photomultiplier tube sensitivity, and thresholds were kept constant for each image sequence. Automated thresholding was performed by normalizing pixel intensity to a decay constant extracted from an intensity histogram of each image. The sum of pixels for each xyz stack was then compared with the sum at baseline. Values are expressed as mean ± SEM. Intragroup and intergroup analyses were performed using a two-tailed Student t test.

Calcium imaging. Time-lapse images of astrocytic Ca^{2+} signals were recorded in the slices every 5 s. Images were acquired 1 min before the solution change as a baseline and 10 min after; 512 × 512 frames were acquired every 5 s using minimal laser power (<40 mW). Changes in Rhod2 intensity ($\Delta F/F_0$) were analyzed using custom-made software (Matlab Inc.) within a manually defined region of interest (10-μm-diameter circle for soma). Relative Rhod2 increases >20% (or >2 SDs) above baseline value were defined as a Ca^{2+} spike. After administration of ATP, the Ca^{2+} response was imaged for 168 s, one frame per 1.12 s, using 512 × 512 frames. Values are expressed as mean ± SEM. Intragroup and intergroup analyses were performed using a two-tailed Student t test.

Drug delivery. For experiments with P2 purinergic receptor antagonists, the slices were exposed to suramin (100 μM; Tocris Bioscience) and PPADS (30 μM; Tocris Bioscience) >30 min before imaging and hypoosmotic challenge. Slices exposed to microinjected ATP were perfused with control aCSF. A fine electrode filled with aCSF containing 500 μm ATP was inserted 40–80 μm into the slice. After a 33.6-s baseline recording, ATP was puffed through the electrode using a Picospritzer (10 psi, 100 ms; Parker Instrumentation); 1% FITC was used to visualize the puff.

ATP Release from Cultured Astrocytes. Serum-free media (control) or solution with 20% reduction in osmolarity (by removing NaCl) was added (400 μL; 2×) to astrocyte cultures derived from WT or *Aqp4*$^{-/-}$ mice. After 15-min exposure, 350-μL samples were collected (450 μL remained in the wells). ATP content in samples collected from cultures grown in 24-well tissue culture plates was measured by using a bioluminescent ATP assay kit (Sigma) and a Victor2 plate reader (Wallac) and was normalized to the cell number (26). A total of eight plates were examined for each genotype and their re-

spective control. Values are expressed as mean ± SEM. Intergroup analyses were done using a two-tailed Student *t* test.

ACKNOWLEDGMENTS. We thank Mr. Justin Chang (University of Rochester Medical Center, Rochester, New York) for making the software used for analyzing astrocytic soma volumes and Ca^{2+} transients, Professor Petter Laake (Institute of Basic Medical Sciences, University of Oslo, Oslo, Norway) for advice on the statistical analysis, and Professor Jeffrey D. Rothstein (Johns Hopkins University, Baltimore) for providing *Glt-1*–EGFP BAC transgenic mice. This work was supported by the US National Institutes of Health Grants P01NS050315 and R01NS056188 (to M.N.), the Research Council of Norway, and the Letten Foundation.

1. Nase G, Helm PJ, Enger R, Ottersen OP (2008) Water entry into astrocytes during brain edema formation. *Glia* 56:895–902.
2. Amiry-Moghaddam M, Ottersen OP (2003) The molecular basis of water transport in the brain. *Nat Rev Neurosci* 4:991–1001.
3. Verkman AS (2009) Knock-out models reveal new aquaporin functions. *Handb Exp Pharmacol* 190:359–381.
4. Nielsen S, et al. (1997) Specialized membrane domains for water transport in glial cells: High-resolution immunogold cytochemistry of aquaporin-4 in rat brain. *J Neurosci* 17: 171–180.
5. Mathiisen TM, Lehre KP, Danbolt NC, Ottersen OP (2010) The perivascular astroglial sheath provides a complete covering of the brain microvessels: An electron microscopic 3D reconstruction. *Glia* 58:1094–1103.
6. Mulligan SJ, MacVicar BA (2006) VRACs CARVe a path for novel mechanisms of communication in the CNS. *Sci STKE* 2006:pe42.
7. Kimelberg HK (2005) Astrocytic swelling in cerebral ischemia as a possible cause of injury and target for therapy. *Glia* 50:389–397.
8. Manley GT, et al. (2000) Aquaporin-4 deletion in mice reduces brain edema after acute water intoxication and ischemic stroke. *Nat Med* 6:159–163.
9. Nagelhus EA, Lehmann A, Ottersen OP (1993) Neuronal-glial exchange of taurine during hypo-osmotic stress: A combined immunocytochemical and biochemical analysis in rat cerebellar cortex. *Neuroscience* 54:615–631.
10. Risher WC, Andrew RD, Kirov SA (2009) Real-time passive volume responses of astrocytes to acute osmotic and ischemic stress in cortical slices and in vivo revealed by two-photon microscopy. *Glia* 57:207–221.
11. Nimmerjahn A, Kirchhoff F, Kerr JN, Helmchen F (2004) Sulforhodamine 101 as a specific marker of astroglia in the neocortex in vivo. *Nat Methods* 1:31–37.
12. Kang J, et al. (2010) Sulforhodamine 101 induces long-term potentiation of intrinsic excitability and synaptic efficacy in hippocampal CA1 pyramidal neurons. *Neuroscience* 169:1601–1609.
13. Regan MR, et al. (2007) Variations in promoter activity reveal a differential expression and physiology of glutamate transporters by glia in the developing and mature CNS. *J Neurosci* 27:6607–6619.
14. Hoffmann EK, Lambert IH, Pedersen SF (2009) Physiology of cell volume regulation in vertebrates. *Physiol Rev* 89:193–277.
15. Kimelberg HK, Macvicar BA, Sontheimer H (2006) Anion channels in astrocytes: Biophysics, pharmacology, and function. *Glia* 54:747–757.
16. Papadopoulos MC, Verkman AS (2005) Aquaporin-4 gene disruption in mice reduces brain swelling and mortality in pneumococcal meningitis. *J Biol Chem* 280:13906–13912.
17. Salter MW, Hicks JL (1994) ATP-evoked increases in intracellular calcium in neurons and glia from the dorsal spinal cord. *J Neurosci* 14:1563–1575.
18. Shao Y, McCarthy KD (1995) Receptor-mediated calcium signals in astroglia: multiple receptors, common stores and all-or-nothing responses. *Cell Calcium* 17:187–196.
19. Wang X, Ge S, Crooks GM (2009) Fluorescent immunohistochemistry and in situ hybridization analysis of pancreas. *Methods Mol Biol* 560:191–201.
20. Amiry-Moghaddam M, et al. (2003) Alpha-syntrophin deletion removes the perivascular but not endothelial pool of aquaporin-4 at the blood-brain barrier and delays the development of brain edema in an experimental model of acute hyponatremia. *Proc Natl Acad Sci USA* 100:2106–2111.
21. Rossi DJ, Brady JD, Mohr C (2007) Astrocyte metabolism and signaling during brain ischemia. *Nat Neurosci* 10:1377–1386.
22. Simard M, Arcuino G, Takano T, Liu QS, Nedergaard M (2003) Signaling at the gliovascular interface. *J Neurosci* 23:9254–9262.
23. Wang X, et al. (2006) Astrocytic Ca2+ signaling evoked by sensory stimulation in vivo. *Nat Neurosci* 9:816–823.
24. Cnaan A, Laird NM, Slasor P (1997) Using the general linear mixed model to analyse unbalanced repeated measures and longitudinal data. *Stat Med* 16:2349–2380.
25. Kang J, Nedergaard M (2000) Imaging astrocytes in acute brain slices. *Imaging Neurons: A Laboratory Manual*, eds Yuste R, Lanni F, Konnerth A (Cold Spring Harbor Laboratory Press, Plainview, NY), pp 1–42.
26. Cotrina ML, et al. (1998) Connexins regulate calcium signaling by controlling ATP release. *Proc Natl Acad Sci USA* 95:15735–15740.